

SIR epidemics with long range infection in one dimension

Peter Grassberger¹

¹JSC, FZ Jülich, D-52425 Jülich, Germany

(Dated: September 8, 2018)

We study epidemic processes with immunization on very large 1-dimensional lattices, where at least some of the infections are non-local, with rates decaying as power laws $p(x) \sim x^{-\sigma-1}$ for large distances x . When starting with a single infected site, the cluster of infected sites stays always bounded if $\sigma > 1$ (and dies with probability 1, if its size is allowed to fluctuate down to zero), but the process can lead to an infinite epidemic for $\sigma < 1$. For $\sigma < 0$ the behavior is essentially of mean field type, but for $0 < \sigma \leq 1$ the behavior is non-trivial, both for the critical and for supercritical cases. For critical epidemics we confirm a previous prediction that the critical exponents controlling the correlation time and the correlation length are simply related to each other, and we verify detailed field theoretic predictions for $\sigma \searrow 1/3$. For $\sigma = 1$ we find generic power laws with continuously varying exponents even in the supercritical case, and confirm in detail the predicted Kosterlitz-Thouless nature of the transition. Finally, the mass $N(t)$ of supercritical clusters grows for $0 < \sigma < 1$ like a stretched exponential. This implies that networks embedded in 1-d space with power-behaved link distributions have infinite intrinsic dimension (based on the graph distance), but are not small world.

I. INTRODUCTION

Epidemic spreading, both on regular lattices and on random graphs, have attracted increasing attention in the statistical physics community [1, 2]. Basically one distinguishes between two types of epidemics. In both all agents except for the *seeds* are susceptible, while infectious agents (such as the seeds in the initial configuration) stay infectious for a finite time (during one time step in the following), which means that they can infect agents that share with them a link. After this infective period, they either become susceptible again (SIS model), or they become “removed”, i.e. either immune or dead (SIR model). In both cases, agents stay at fixed places (whence they can be identified with lattice sites or network vertices), so that the entire dynamics is contained in the changes of their internal (S, I, R) states.

There exist of course several generalizations of these two basic schemes (e.g. cooperative infection [3, 4], infection using the “power of choice” [5], moving agents [6], memory effects [7], etc.), but even the basic schemes show rich behavior, if we allow for different network topologies.

In the following we shall only deal with basic SIR epidemics, with discrete time and infective period equal to one time step. In this case, the process must die out on any finite system, since susceptibles are used up but not replenished, and the set of “removed” sites becomes, for large times, just a percolation cluster. More precisely, we shall discuss two models, both of which involve infection over large distance, with the infection probability decaying as some inverse power of the distance [8–10]. In both, the sites can be viewed as sites in an infinitely large 1-d lattice (in the simulations we use $L = 2^{64}$ sites, which is big enough so that we never have to worry about finite size effects, except in a few cases pointed out later [11]). In both models, each infected site first attempts to infect k_0 other sites (and succeeds so with probability 1, if these sites are still susceptible), and then attempts with

probability p to infect one more site. Thus, the average number of newly attempted infections per node, which is also equal to the average out-degree of the generated graph, is

$$k_{\text{out}} = k_0 + p. \quad (1)$$

But both models differ slightly in how these sites are connected, i.e. how the attempted infections are chosen:

- In model (A) we assume that in each attempt the target site is chosen randomly, with a distance $\pm x$ from the infectious site that is distributed according to a power law,

$$P(x) \sim x^{-\sigma-1} \quad (2)$$

for large x . More precisely, this distribution is obtained by first drawing a real-valued random number y uniformly from the interval $(1/L^\sigma, 1]$ (for $\sigma > 0$), $[1, 1/L^\sigma)$ (for $\sigma < 0$) or $[0, \ln L]$ (for $\sigma = 0$) and setting

$$x = \begin{cases} \lfloor y^{-1/\sigma} \rfloor & \text{for } \sigma \neq 0, \\ \lfloor e^y \rfloor & \text{for } \sigma = 0. \end{cases} \quad (3)$$

Notice that we do *not* check that all attempts try to infect different targets. If several attempts are aimed at the same target, all except the first one are simply lost.

- In model (B) we first infect the left and right neighbors, and only in the subsequent infections distant sites are chosen, again with the same probability $P(x)$ given above.

In model (A), it can happen that *all* attempts during one time step try to infect target sites that are no longer susceptible, in which case the epidemic dies. This cannot happen in model (B). There, the right neighbor of the

rightmost infected site is always susceptible, as is also the left neighbor of the leftmost site. Model (B) is indeed, as far as the geometric structures obtained for $t \rightarrow \infty$ are concerned, a modification of the Watts-Strogatz [12] small world model that was studied previously in [13–18].

In the next section, we will discuss the most important features common to both models. In Sec. III we shall treat in more detail the case $\sigma = 1$, where we find a number of non-trivial exact results. The critical case of model (A) with $0 < \sigma < 1$ is studied in Sec. IV [model (B) is always supercritical, as it never can die, thus no critical phase exists]. The supercritical case for $0 < \sigma < 1$ is finally discussed in Sec. V. The paper concludes with a discussion in Sec. VI.

II. GENERAL FEATURES

We always start with a single seed located at the origin, $x = 0$. Boundary conditions are periodic. The jump probability $P(x)$ is cut off at $x = L$, i.e. the length of the widest jumps allowed is precisely the lattice size. The distribution of infected (or “active”, as we shall call them in the following) sites at time $t \geq 0$ is denoted as $\rho(x, t)$. The distribution of removed sites is then

$$R(x, t) = \sum_{t'=0}^{t-1} \rho(x, t'). \quad (4)$$

The average number of active sites at time t is then

$$n(t) = \sum_x \rho(x, t), \quad (5)$$

while the number of immune sites is

$$N(t) = \sum_x R(x, t) = \sum_{t'=0}^{t-1} n(t'). \quad (6)$$

Notice that $N(t) + n(t)$ can also be interpreted as the average number of sites reached by chains of at most t links from a randomly chosen pivot. Therefore, if $N(t) \sim t^D$, the exponent D would be the intrinsic (or “topological” [19][20]) dimension of the final network.

For model (B), $R(x, t) = 1$ and $\rho(x, t) = 0$ for all $|x| < t$. Thus the active sites form two outgoing waves, one moving to the right and the other to the left. For $\sigma > 0$ the infection is sufficiently short ranged that these two waves don’t interfere with each other, in the limit $t \rightarrow \infty$. Basically the same is also true for model (A), although in that case $R(x, t)$ and $\rho(x, t)$ are no longer strictly 1 and 0, respectively, for $|x| < t$. Nevertheless, activity dies out also there for any finite x , i.e. $\rho(x, t) \rightarrow 0$ for $t \rightarrow \infty$.

This scenario no longer holds for $\sigma < 0$ (for the case $\sigma = 0$ see [15]). In that case, $P(x)$ would not be normalizable for infinitely large lattices, hence finite lattice effects become important. Indeed, on large but finite lattices, both $R(x, t)$ and $\rho(x, t)$ become uniform, see Fig. 1.

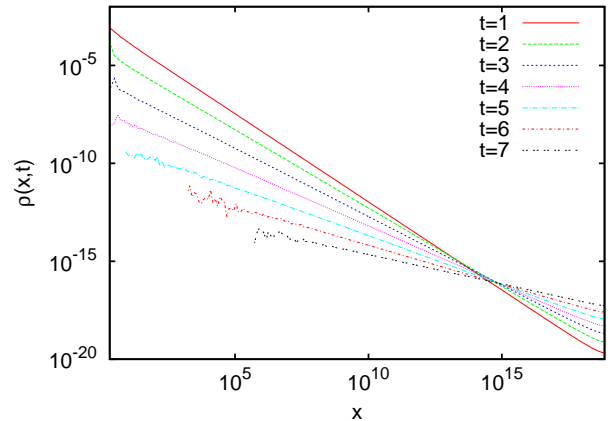


FIG. 1. (Color online) Densities of active sites at times $t = 1, 2, \dots, 7$ for model (A) with $\sigma = -0.1$, $k_0 = 2$, and $p = 1$, i.e. with exactly 3 offsprings per active site. Because of left-right symmetry, we show here and in the following plots only the distribution for $x > 0$. The densities become more and more uniform for increasing t , showing the mean field nature when $\sigma < 0$.

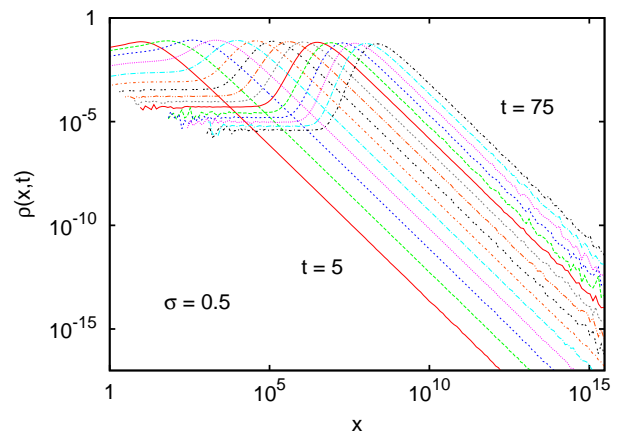


FIG. 2. (Color online) Densities of active sites at times $t = 5, 10, \dots, 75$ for model (A) with $\sigma = 0.5$, $k_0 = 1$, and $p = 1$, i.e. with exactly 2 offsprings per active site. Notice the tails decaying $x^{-\sigma-1}$ for all times. For small x the activity dies out because (i) the density of immune sites gets higher and higher, and (ii) the parent activity shifts more and more outside.

Also, the formation of finite loops is suppressed by powers of L (the number of loops with m links, each limited in length to less than some constant, scales as $L^{1+m\sigma}$), so that the cluster of immunes becomes locally tree like in the limit $L \rightarrow \infty$ and the model becomes of mean field type.

In contrast, for $\sigma > 0$ it is found that both $R(x, t)$

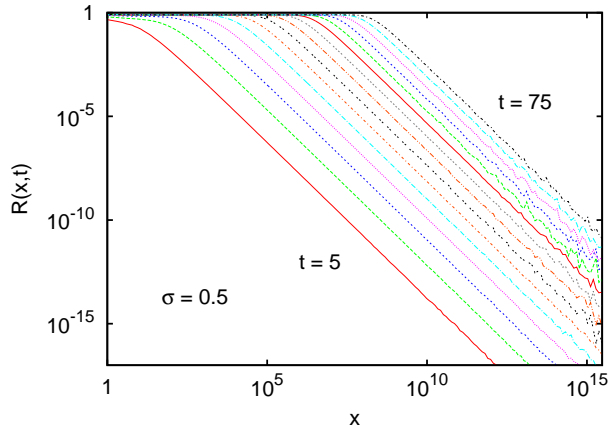


FIG. 3. (Color online) Densities of immune sites at the same times as in Fig. 2.

and $\rho(x, t)$ decay asymptotically as $|x|^{-\sigma-1}$ for all times $t \geq 0$, see e.g. Figs. 2, 3 (see also [21]). This is easily understood. First of all, they cannot decay faster, since the offspring distribution of a population concentrated at the origin would decay like that and any smearing due to a finite extend of the parent population can only make the offspring distribution wider. On the other hand, if $\rho(x, t)$ decays at some given time t not slower than $|x|^{-\sigma-1}$, then the distribution of its offsprings is given for sufficiently large $|x|$ by

$$\rho(x, t+1) \approx \sum_y \rho(y, t) P(x-y) \sim |x|^{-\sigma-1}. \quad (7)$$

In this expression we have neglected saturation effects (not all infections are successful, because not all sites are susceptible), but this approximation should be correct for large $|x|$ where most of the sites *are* susceptible. Since $R(x, t)$ is just a sum over $\rho(x, t')$ with $t' < t$, it satisfies the same asymptotic behavior.

Notice that this argument only tells about the limit where we first let $x \rightarrow \infty$, and then let t become large. It does not prove that $R_\infty(x) = \lim_{t \rightarrow \infty} R(x, t)$ and $\rho_\infty(x) = \lim_{t \rightarrow \infty} \rho(x, t)$ decay asymptotically as $|x|^{-\sigma-1}$. For $0 < \sigma \leq 1$ this seems to be correct nevertheless (see Figs. 2,3), but it does not hold for $\sigma > 1$. In that case the process dies with probability one for model (A) (for an elegant and simple proof, see [22]), but it survives forever for model (B). In the latter case the average number of active sites, $n(t) = \sum_x \rho(x, t)$, tends to a constant and the wave of active sites has a stationary profile in a co-moving frame (in a frame moving with constant velocity the profile widens due to fluctuations of the velocity). Profiles $R(x, t)$ are shown in Fig. 4 for model (B) with $\sigma = 1.5$ and one long-range contact per site. We see that the tails decay $\sim |x|^{-\sigma-1}$ for all finite times, but that this behavior sets in later and later for increasing t . The

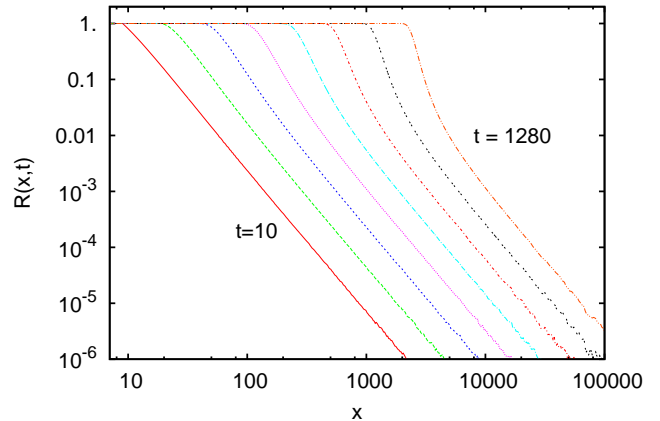


FIG. 4. (Color online) Densities of the immune cluster at times $t = 10, 20, 40, \dots, 1280$ for model (B) with $\sigma = 1.5$, $k_0 = 3$, and $p = 1$, i.e. with two local and one long-range offsprings. For large x , all densities decay $\sim 1/x^{\sigma+1}$, but for large times this tail sets in later and later.

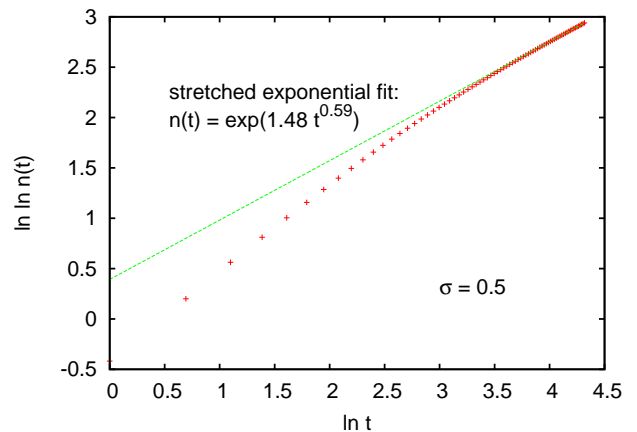


FIG. 5. (Color online) Plot of $\log \log n(t)$ versus $\log t$, where $n(t)$ is the average number of active sites, for the same run shown also in Figs. 2 and 3. The straight line represents a stretched exponential fit to the data with $50 \leq t \leq 75$, corresponding to $2.6 \times 10^6 \leq n(t) \leq 1.6 \times 10^8$. Statistical errors are much smaller than the symbols.

bulk of the outgoing wave has finite width (i.e., becomes increasingly sharper in a log-log plot such as Fig. 4). In the terminology of [23], the fronts for model (B) are *pushed* when $\sigma > 1$.

The same is true for model (A), although one has to condition on (exponentially rare) surviving events in order to see this. This could be done by using e.g. PERM [24], but we have not done it.

Notice that the times in Fig. 4 are exponentially in-

creasing. The linear progression of the front in the log-log plot then means that the immune cluster travels at constant speed. This is in contrast to the case $\sigma < 1$ shown in Figs. 2 and 3 (where time increases linearly between successive curves). There the wave of infection travels with a speed that increases faster than a power with time, in agreement with [21, 25] but in contrast to [26]). On the other hand, the decreasing distances between successive curves in Figs. 2 and 3 show that this increase of speed is less than exponential, in contrast to [21, 25]. In order to see this more clearly, we plot $n(t)$ in Fig. 5 for the runs shown in Figs. 2, 3. More precisely, Fig. 5 shows $\log \log n(t)$ plotted against $\log t$. An exponential $n(t) \sim \exp(at)$ would correspond in this plot to a straight line with slope 1. This is obviously not observed (statistical errors are smaller than the symbol sizes). Rather, the data for large t suggest a stretched exponential $n(t) \sim \exp(at^\gamma)$ with $\gamma = 0.59(1)$. But we should be careful in accepting this fit as the true asymptotic scaling. First of all, the data in Fig. 2 are slightly curved, even for the largest t , suggesting that this estimate of γ is too high. Also, fitting stretched exponentials is notoriously fraught with uncertainties. The same behavior is also seen for model (B) (data will be shown later). It shows also that the mass of clusters with diameter ℓ increases slower than exponentially with ℓ , in contrast to claims made in [16] (exponential increase is of course seen in the mean field regime, $\sigma < 0$). More details will be given in Sec. V.

III. THE CASE $\sigma = 1$

It is well known that the case of interacting Levy flights with $\sigma = 1$ is very special, in particular in one dimension of space. This was first found by Dobrushin, Ruelle [27], and Dyson [28] who showed that 1-d Ising models with long range interactions can only have a finite temperature phase transition, if $\sigma \leq 1$. Very soon after this, Anderson et al. [29] and Thouless [30] showed that for $\sigma = 1$ one not only does have a phase transition, but that this transition is similar to the Berezinskii-Kosterlitz-Thouless (BKT) transition in displaying a region with generic power laws in the supercritical phase with σ -dependent exponents. As in the XY model, the reason is that configurations can be described as organized by defects which interact with each other by an attractive logarithmic potential. This argument was later extended by Cardy [31] to Potts and other models. Due to the Fortuin-Kasteleyn [32] relationship between the Potts model and percolation [31], this applies also to percolation and thus also to SIR epidemics. But it seems that the consequences for the latter have never been worked out in detail, with one notable exception: It was shown in [33] that the percolation transition for $\sigma = 1$ is discontinuous in the sense that the order parameter (the density of infected sites for $t \rightarrow \infty$) jumps discontinuously, when p is increased through the percolation threshold. This might seem con-

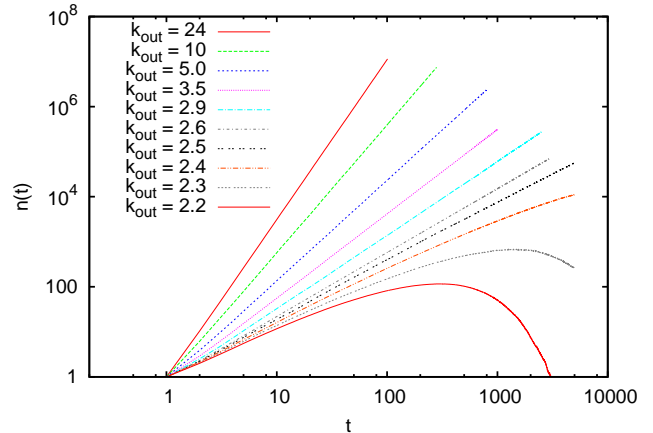


FIG. 6. (Color online) Log-log plot of $n(t)$ versus t for model (A) with $\sigma = 1$, and for different values of k_{out} . All curves for $k_{\text{out}} \geq 2.6$ seem to become asymptotically straight, giving a rough estimate of $k_{\text{out}} = 2.6(1)$ for the critical point.

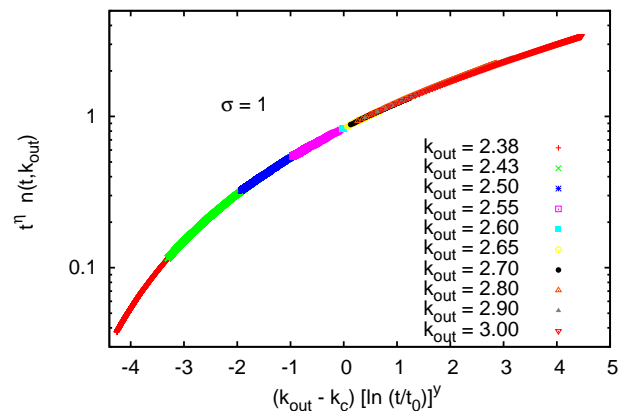


FIG. 7. (Color online) Data collapse for model (A), using the finite- t scaling ansatz Eq. (11). Parameters are $k_c = 2.602$, $\eta = 1.42$, $t_0 = 0.88$, and $y = 1.37$. Only points with $t \geq 3$ are plotted.

tradictory to the claim of universal power laws (which usually hold only at continuous phase transitions), but several similar “hybrid” cases, where aspects typical of a first order transition coexist with aspects of a second order transition, have been found recently also in other contexts [4, 34].

Numerical results for the increase of $n(t)$ in both models at $\sigma = 1$ are shown in Figs. 6 to 8. From Fig. 6 we see that model (A) exhibits indeed generic power law behavior (in agreement with the predictions of [29–31]) for

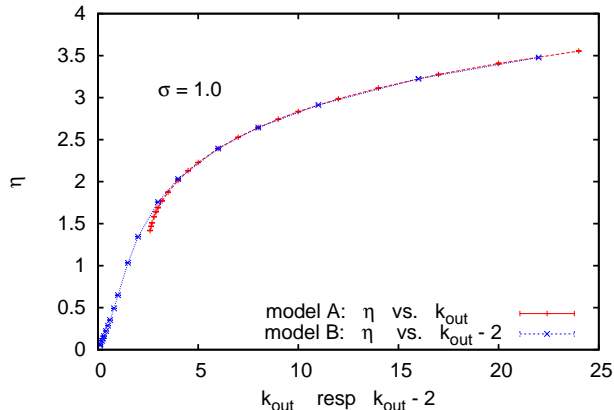


FIG. 8. (Color online) Exponents $\eta(k_{\text{out}}, \sigma = 1)$ governing the increase of active sites obtained from Figs. 6 and 9. For both models, η is plotted against the number of *long-range* outgoing links, i.e. it is plotted against k_{out} for model (A) and against $k_{\text{out}} - 2$ for model (B).

all $k_{\text{out}} > k_c$, where $k_c \approx 2.6(1)$:

$$n(t, k_{\text{out}}) \sim t^{\eta(k_{\text{out}})}. \quad (8)$$

At the critical point, a straightforward fit gives $\eta \equiv \eta(k_{\text{out}}) = 1.42(4)$.

More precise determinations of k_c and η are possible by using the finite (cluster-)size scaling expected for BKT transitions. Let us define $\varepsilon = k_{\text{out}} - k_c$. Near the critical point there exists a characteristic time scale $\tau(\varepsilon)$ which diverges as $\varepsilon \rightarrow 0$. Inversely, we can for each t define an effective distance from the critical point as $\epsilon(t)$. Using the latter we can make the finite-time scaling (FTS) ansatz

$$n(t, k_{\text{out}}) \sim t^{\eta} g[\varepsilon/\epsilon(t)], \quad (9)$$

where $g(z)$ is an analytic function joining smoothly the sub- and supercritical regions. While this ansatz is common to models with short and long range infections, the scaling of $\epsilon(t)$ in the limit $t \rightarrow \infty$ is different. For short range contacts it is a power law, while for a BKT transition we expect

$$\epsilon(t) \sim \left[\ln \frac{t}{t_0} \right]^{-y}. \quad (10)$$

Equations (9) and (10) can be combined to

$$n(t, k_{\text{out}}) \sim t^{\eta} g[(k_{\text{out}} - k_c) (\ln \frac{t}{t_0})^y]. \quad (11)$$

A data collapse based on Eq. (11) is shown in Fig. 7. We see a nearly perfect collapse (only points with $t \geq 3$ are plotted), giving our best estimates

$$k_c = 2.60(1), \quad \eta = 1.42(1), \quad t_0 = 0.9(1) \quad \text{and} \quad y = 1.37(3). \quad (12)$$

TABLE I. Exponents $\eta(k_{\text{out}})$ for model (B). Column 2 gives our results, column 3 is from Table 1 of [18], noticing that $d_g = 1 + \eta$ and $\beta = (k_{\text{out}} - 2)/2$.

k_{out}	η (this work)	η (Ref. [18])
2.1	0.0513(2)	
2.2	0.1048(3)	0.1038(24)
2.3	0.1625(4)	
2.4	0.2226(4)	0.2121(44)
2.5	0.2855(6)	
2.6	0.3524(7)	0.3532(74)
2.8	0.4963(7)	0.4992(67)
3.0	0.6492(6)	0.656(8)
3.5	1.0330(17)	
4.0	1.344(2)	1.347(16)
5.0	1.757(4)	1.770(23)
6.0	2.032(4)	
8.0	2.394(6)	
10.0	2.646(7)	
13.0	2.913(9)	
18.0	3.224(13)	
24.0	3.478(12)	

To our knowledge, neither η nor y have been calculated before. We conjecture that they are universal for all models where $P(x) \sim 1/x^2$ asymptotically and where, in contrast to model (B), the epidemic can die (we made also preliminary simulations of a generalization of model (B) where left and right neighbors are infected with probabilities 0.9. The results support the conjecture). Our value of k_c is consistent with the exact bound $k_c \geq 2$ [33] for this class of models.

Combining Eqs. (8) and (11) gives that $g(z)$ behaves for large z as a stretched exponential, $\ln g(z) \sim z^{1/y}$, and that

$$\eta(k_{\text{out}}) - \eta \sim (k_{\text{out}} - k_c)^{1/y}. \quad (13)$$

This is reasonably well satisfied.

As seen from Fig. 9, essentially the same behavior is found also for model (B), with one important exception: Since model (B) with $\sigma \geq 1$ is supercritical for all $k_{\text{out}} > 2$, all curves become straight lines for $t \rightarrow \infty$ and $\eta(k_{\text{out}})$ tends to zero for $k_{\text{out}} \rightarrow 2$. The dependence of $\eta(k_{\text{out}})$ on k_{out} is shown in Fig. 8 and Table 1. The fact that $n(t, k_{\text{out}})$ increases as a power of t is indeed known [15, 18]. In [15] exact upper bounds on $\eta(k_{\text{out}})$ were given for small k_{out} , and these were compared to simulation results in [18]. When comparing our estimates with the results of [18], we should notice that $1 + \eta$ is the graph dimension of the cluster of immunes, and that the constant β used in [18] corresponds to $(k_{\text{out}} - 2)/2$. From Table 1 we see that our data are roughly 10 times more precise, but otherwise they are in very good agreement.

For both models η becomes the same for large k_{out} , which is to be expected: For large k_{out} , the evolution

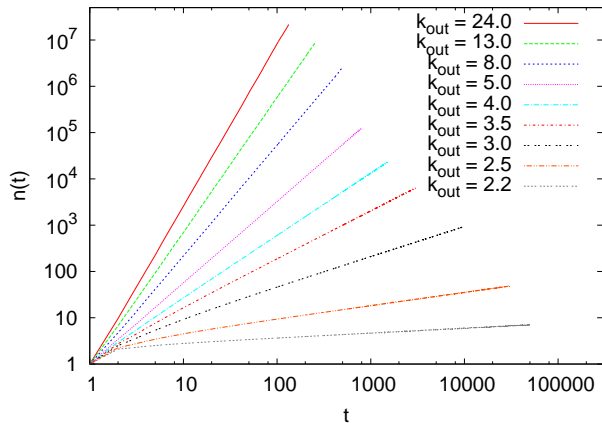


FIG. 9. (Color online) Same as Fig. 6, but for model (B). Since model (B) is supercritical for all $k_{\text{out}} > 2$, all curves now become straight lines for $t \rightarrow \infty$.

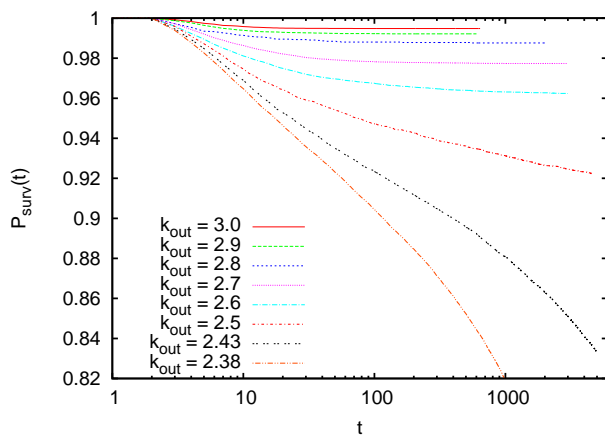


FIG. 10. (Color online) Log-linear plot of $P_{\text{surv}}(t)$, the probability that there are still some active sites at time t , for model (A) with $\sigma = 1$. All curves for $k_{\text{out}} \geq k_c$ (including the critical one!) seem to become horizontal with $P_{\text{surv}}(\infty) > 0$.

mainly depends on long range infections, as infections between nearest neighbors just fill in gaps in the cluster of immunes. It seems that $\eta \sim \log k_{\text{out}}$ for large k_{out} , so that $n(t) \sim \exp(\ln k_{\text{out}} \ln t)$. More precisely, both data sets are very well fitted by $\eta = 0.9 + 0.84 \ln(k_{\text{out}} - k_{\text{out,short}})$, where $k_{\text{out,short}}$ is the number of short-range infections. We have no theoretical argument for this.

Survival probabilities $P_{\text{surv}}(t)$ for model (A) are shown in Fig. 10. As expected, they all tend to constants when the process is supercritical. More surprising, it seems that also for the critical case $k_{\text{out}} = k_c = 2.6$ we have $P_{\text{surv}}(t) \rightarrow \text{const}$ for $t \rightarrow \infty$. Indeed, even in the clearly

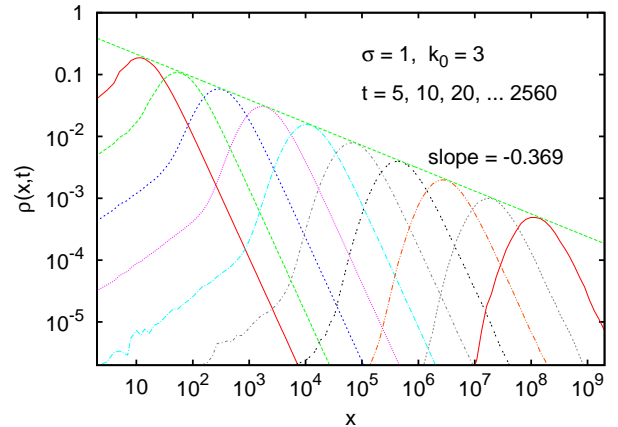


FIG. 11. (Color online) Log-log plot of the densities of active sites for model (A) with $\sigma = 1$ and $k_0 = 3$, for times $t = 5, 10, \dots, 2560$.

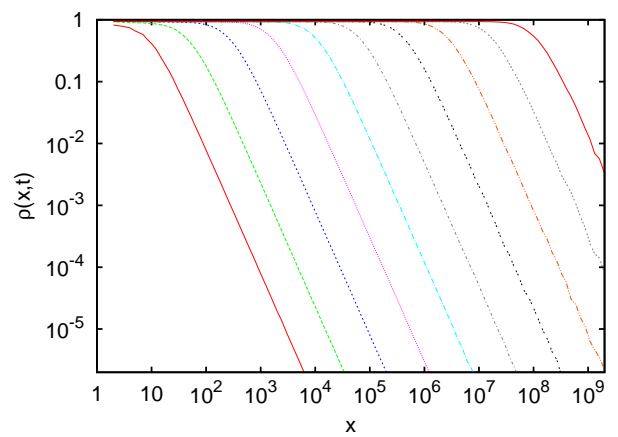


FIG. 12. (Color online) Log-log plot of the densities of immune sites for model (A) with the same parameters as in Fig. 11.

subcritical case $k_{\text{out}} = 2.4$, we see that $P_{\text{surv}}(t)$ first curves upward, before it finally goes to zero. This is in contrast to the behavior of SIR epidemics with short range contacts, but it is precisely what was proven rigorously in [33]: When $\sigma = 1$, the percolation transition is discontinuous in the sense that the order parameter (which is just $\lim_{t \rightarrow \infty} P_{\text{surv}}(t)$) jumps discontinuously when the control parameter k_{out} passes through the critical point. Furthermore, $P_{\text{surv}}(\infty) > 2/k_c$ as predicted in [33].

Spatial distributions of active and immune sites for model (A) are shown in Figs. 11 and 12. Superficially, these distributions look similar to those for the supercrit-

ical case with $\sigma < 1$ shown in Figs. 2 and 3, but there are important differences:

- The curves are now equidistant for exponentially increasing times, corresponding to the fact that the number of active sites, the number of immune sites, and the effective radius all increase like powers of t , while they increased faster than polynomial when $\sigma < 1$.
- While the peaks in Fig. 2 become narrower with increasing t , now the shapes of the curves are independent of t , suggesting finite time scaling for $\sigma = 1$, but not for $\sigma < 1$. This is also seen by making formal data collapses (not shown here).

In view of the fact that $R(x, t)$ is constant (t -independent) for small values of x we make for $\sigma = 1$ and $k_{\text{out}} \geq k_c$ the ansatz

$$R(x, t) \approx \phi(x/\xi(t)) \quad (14)$$

for $t \rightarrow \infty$, with

$$\phi(z) = \begin{cases} \text{const} & \text{for } |z| \ll 1, \\ |z|^{-\sigma-1} & \text{for } |z| \gg 1. \end{cases} \quad (15)$$

and $\xi(t) \rightarrow \infty$ for $t \rightarrow \infty$. From this ansatz follows immediately that $\xi(t)$ has to scale exactly like $N(t)$,

$$\xi(t) \sim t^{1+\eta}, \quad (16)$$

and that the density of active sites satisfies the scaling

$$\rho(x, t) \approx t^{-1} \psi(x/\xi(t)) \quad (17)$$

with $\psi(z) = z\phi'(z)$.

- Since, according to Eqs.(17) and (16), both the peak heights and the peak positions of $\rho(x, t)$ scale as powers of t for $\sigma = 1$, also the peak heights must scale as a power of the positions,

$$\rho_{\text{max}}(t) \equiv \max_x \rho(x, t) \sim \xi(t)^{-1/(1+\eta)}. \quad (18)$$

This is clearly seen in Fig. 11, where we obtain $1/(1+\eta) = 0.369(3)$ or $\eta = 1.71(2)$, in perfect agreement with the direct measurement $\eta = 1.692(6)$. But as we shall see later, Eq. (18) does not hold for $\sigma < 1$.

Since the generated clusters are basically compact, we can measure η also by measuring the average of $\log|x|$, either over the active or over the immune sites. Both averages should scale as $\log \xi(t) \approx (1+\eta) \log t$. This was indeed verified numerically.

Equations (14) to (18) were also tested for several other values of k_{out} , and were satisfied in all cases. This includes even the critical case k_c . Also there, $R(x, t)$ is flat for $x \ll \xi(t)$, showing that the pair connectedness does

not decrease as long as $x < \xi(t)$. This is of course in agreement with the result that P_{surv} does not decrease to zero at the critical point, and that the percolation transition is discontinuous for $\sigma = 1$ [33].

We should point out that Eqs. (14) to (18) hold also for model (B) if $\sigma = 1$, although finite time corrections are somewhat larger since not all links are distributed according to a power law. For one typical case ($k_{\text{out}} = 3.0$), see Fig. 13. In spite of the visible deviation in the curve for $t = 20$, the peaks line up for larger t along a perfect power law, with $\eta = 1 - 1/0.610(4) = 0.64(1)$. This should be compared to $\eta = 0.6484(4)$ from the direct measurement of $n(t)$.

Finally, let us discuss the predictions of mean field theory for the case $\sigma = 1$. The exact evolution for $R(x, t)$ can be written as

$$R(x, t+1) = R(x, t) + \sum_y P(x-y) \langle n_{\text{act}}(y, t)(1 - n_{\text{immune}}(x, t)) \rangle, \quad (19)$$

where $n_{\text{act}}(x, t)$ and $n_{\text{immune}}(x, t)$ are the exact fluctuating densities of active and immune sites, and angular brackets indicate an ensemble average. The mean field assumption is

$$\begin{aligned} \langle n_{\text{act}}(y, t)n_{\text{immune}}(x, t) \rangle &= \\ &= \langle n_{\text{act}}(y, t) \rangle \langle n_{\text{immune}}(x, t) \rangle \\ &= \rho(x, t)R(x, t). \end{aligned} \quad (20)$$

Inserting this and the scaling ansatzes into the r.h.s. of Eq.(20), we find that it gives back the scaling ansatz for the l.h.s., i.e. our scaling assumptions are consistent with mean field theory. In contrast, the scaling ansatzes would not be compatible with this mean field theory, if $\sigma \neq 1$.

IV. THE CRITICAL MODEL (A) FOR $0 < \sigma < 1$

Critical percolation with long range infection has been studied both by means of field theory [9, 10] and by means of simulations [10]. The field theoretic analysis (using the epsilon expansion) should hold in d dimension of space for any d , provided $\sigma \approx d/3$ [9, 10] – thus it should also be applicable to $d = 1$, provided $\sigma \approx 1/3$. Remarkably, it predicts that mean field theory does not only hold for $\sigma < 0$ (where it holds for the supercritical case), but also for $0 < \sigma < 1/3$. It also predicts, for $d \geq 2$, the value of σ above which short range behavior should be observed. Again it is remarkable that this value is not where short range behavior is observed in the supercritical case ($\sigma = d$), but at a smaller value of σ [10].

While these predictions have been reasonably well confirmed for $d = 2$ [10] (much larger simulations, again on lattices with 2^{64} sites, will be published elsewhere [35]), it seems that no simulations were yet done for $d = 1$.

The most obvious strategy for finding the critical values k_c of k_{out} is to start again from a single seed and

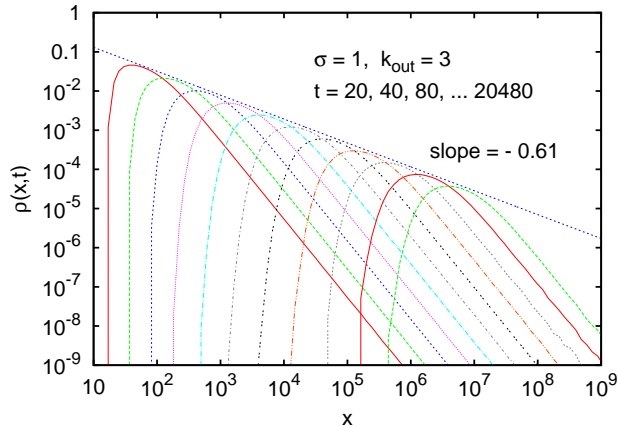


FIG. 13. (Color online) Log-log plot of the densities of active sites for model (B) with $\sigma = 1$ and $k_{\text{out}} = 3$, for times $t = 20, 40, \dots, 20480$. Compared to Fig. 11, the curves for the smallest t values now show less perfect scaling.

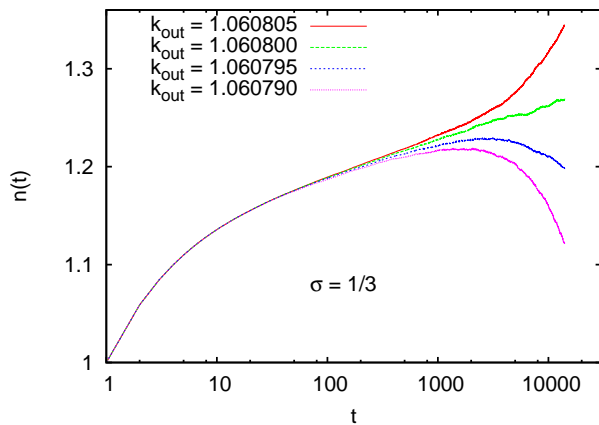


FIG. 14. (Color online) Log-linear plot of $n(t)$ for model (A) with $\sigma = 1/3$ and $k_{\text{out}} \approx k_c$. These data are compatible with $k_c = 1.06799(1)$ and $\eta = 0$, if we allow for logarithmic corrections, $n(t) \sim [\ln t]^\alpha$ with $\alpha \approx 0.5$ to 1.

to look for the best scaling behavior $n(t) \sim t^\eta$ in the large- t limit. In general this works without too many problems, but we have to expect large finite- t corrections near any change of the critical behavior, i.e. in particular near $\sigma = 1/3$ and near $\sigma = 1$. But one must be aware of surprises. As two examples we show $n(t)$ versus t for $\sigma = 1/3$ (where we expect $\eta = 0$, but slow convergence due to possible logarithmic corrections) and for $\sigma = 0.4$, where we should a priori expect much less problems. The data, based on simulations of typically $\approx 10^8$ clusters, are shown in Figs. 14 and 15. While Fig. 14 is compatible

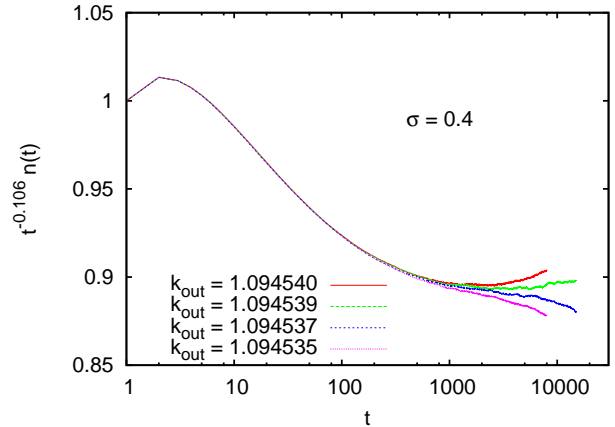


FIG. 15. (Color online) Log-linear plot of $t^{-0.106} n(t)$ for model (A) with $\sigma = 0.4$ and $k_{\text{out}} \approx k_c$. These data are compatible with $k_c = 1.094538(2)$ and $\eta = 0.105(3)$. The main uncertainty of η comes from the obvious corrections to scaling. Notice, however, the expanded y -scale. Notice also that finite (lattice) size corrections are negligible in these simulations, even for the largest values of t . Thus, in order to obtain the true critical exponents, one should take the large- t behavior serious, and should not try to fit in an intermediate region of t .

with nothing more than the expected logarithmic corrections, the corrections to scaling seen in Fig. 15 are much more complicated. They cannot be described by a single power term, and they contribute most to the uncertainty of our estimate of η .

Plots similar to Figs. 14 and 15 were also made for several other values of σ . In addition to $n(t)$, we also looked in the same way at $P_{\text{surv}}(t)$ (plots not shown), for which we assumed

$$P_{\text{surv}}(t) \sim t^{-\delta}. \quad (21)$$

Results are shown in Figs. 16 to 18. They first of all confirm the prediction that mean field behavior holds for all $\sigma < 1/3$, not only for $\sigma < 0$ as in the supercritical case. The critical values of k_{out} converge to $k_c \rightarrow 1$ for $\sigma \rightarrow 0$. Both k_c and η seem to reach their limits for $\sigma \rightarrow 1$ with infinite slope, $\lim_{\sigma \rightarrow 1} dk_c/d\sigma = \lim_{\sigma \rightarrow 1} d\eta/d\sigma = \infty$. This is to be expected, since both can be viewed as infinite for $\sigma > 1$: There, the epidemic dies out for any finite value of k – but as k is increased, the mass increases during the transient faster than any power. We also see, in agreement with the last section, that $\delta \rightarrow 0$ when $\sigma \rightarrow 1$. On the basis of Fig. 18 we conjecture more precisely that $\delta \approx 1 - \sigma$ when $\sigma \rightarrow 1$. Finally we compare to the predictions of [9], represented in Figs. 17 and 18 by straight lines. These predictions are based on an ϵ -expansion with $\epsilon = d - 3\sigma$. Although this expansion is most likely only asymptotic, it should give correct results when $\epsilon \rightarrow 0$. This is definitely the case for Fig. 17, where

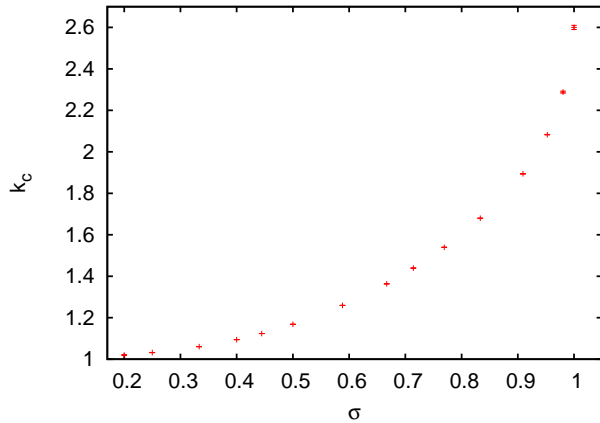


FIG. 16. (Color online) Values of k_c versus σ for critical model (A). For small σ the values approach the value $k_c \rightarrow 1$ for branching processes. For $\sigma \rightarrow 1$ the value $k_c = 2.60(1)$ obtained in the last section is reached with an infinite slope.

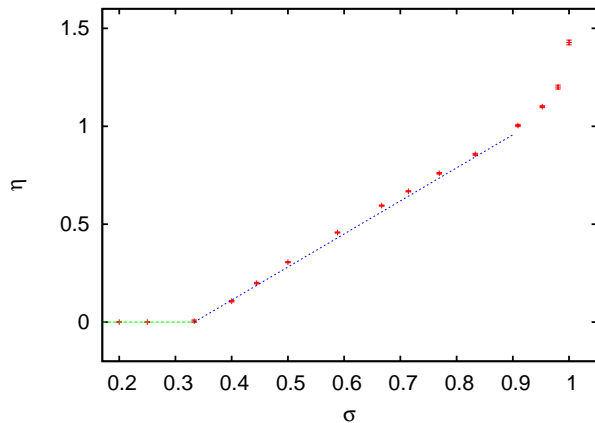


FIG. 17. (Color online) Exponents $\eta(\sigma)$, defined via $n(t) \sim t^\eta$, versus σ for critical model (A). The horizontal line is the mean field prediction $\eta = 0$ for $\sigma < 1/3$. The straight tilted line is the prediction of [9] that should be exact for σ slightly above $1/3$. Finally for $\sigma = 1$ we have the value $\eta = 1.428(12)$ obtained in Sec. III.

the prediction seems to be valid up to $\sigma \approx 1$. For δ the agreement is much worse. Even for $\sigma = 0.4$ it gives a prediction for $1 - \delta$ that is too large by ≈ 15 per cent. This might be related to the anomaly seen in Fig. 15, and might indicate that we have still underestimated finite- t corrections in the regime $1/3 < \sigma < 1/2$. The latter is also suggested by the slight disagreement in the region $1/3 < \sigma < 1/2$ with Eq. (33).

For SIR epidemics with short range infection, one can

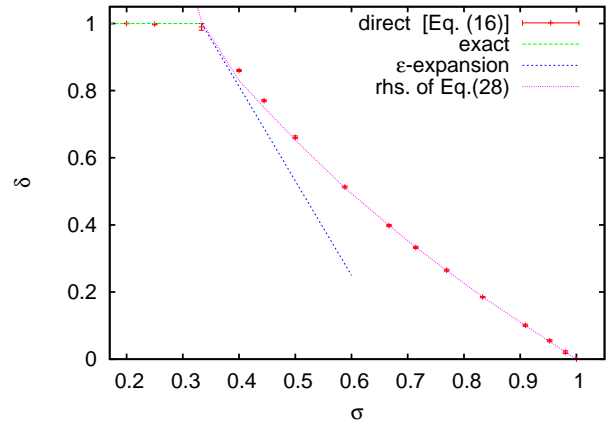


FIG. 18. (Color online) Exponent δ versus σ for critical model (A). The points with error bars are obtained directly from the definition $P_{\text{surv}}(t) \sim t^{-\delta}$, while the dotted curve is obtained from the data shown in Fig. 17, using Eq. (33). Again the straight lines are the exact mean field prediction (for $\sigma < 1/3$) and the epsilon expansion result of [9] (for σ slightly above $1/3$).

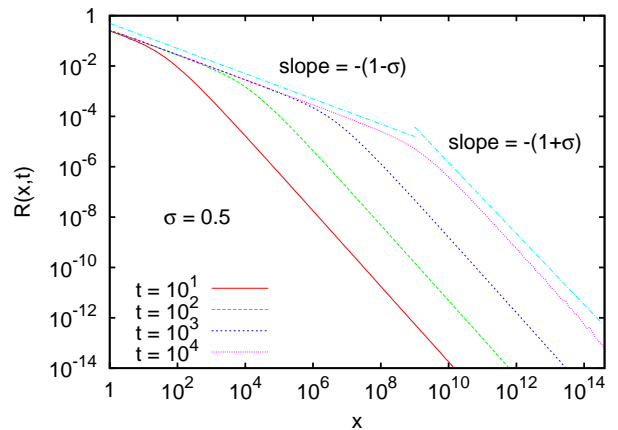


FIG. 19. (Color online) Densities of immune sites for critical epidemics with $\sigma = 1/2$, for $t = 10, 10^2, \dots, 10^4$. For large x all curves show the by now well known tail $R \propto 1/x^{1+\sigma}$, but for smaller values of x the flat part seen in Figs. 3, 4 and 11 is replaced by a power law $R \propto 1/x^{1-\sigma}$.

also define a critical exponent z that describes how the correlation length increases with time, $\xi \sim t^z$. Figure 19 suggests that there is indeed a well defined diverging length scale (the location where the break of slopes occurs; notice that this length scale should be defined by geometric averaging [8], instead of the arithmetic averaging usually taken for short range infects – characterizing

length scales by arithmetic averages when $\sigma < 1$, as done e.g. in [19], can lead to dubious results). In that figure we present the densities of immune sites for different values of t , for one randomly picked value of σ . The data shown in Fig. 19 are for $\sigma = 1/2$, but similar results were found for all other $0 < \sigma < 1$. In particular, in all cases we see two different powers for $x < \xi(t)$ and $x > \xi(t)$.

More precisely, we observe the by now well known tail $R(x, t) \propto 1/x^{1+\sigma}$ for large x , but for small x we observe a completely new phenomenon. Instead of the flat parts seen in Figs. 3, 4 and 11 for small x we now see another power law,

$$R(x, t) \propto 1/x^{1-\sigma}, \quad (22)$$

for $x < \xi(t)$, where $\xi(t)$ is a function that increases like a power for large t ,

$$\xi(t) \sim t^z. \quad (23)$$

Indeed, data collapses (not presented here) show that $R(x, t)$ satisfies a scaling law similar to Eq. 14,

$$R(x, t) = x^{\sigma-1} \Phi(x/\xi(t)), \quad (24)$$

where

$$\Phi(x) = \begin{cases} \text{const} & \text{for } |x| \ll 1, \\ |x|^{-2\sigma} & \text{for } |x| \gg 1. \end{cases} \quad (25)$$

It is not difficult to relate the exponent z to the exponent η . Indeed, by summing $R(x, t)$ over all x we obtain

$$\begin{aligned} N(t) &= \sum_x R(x, t) \\ &\approx \int_0^{\xi(t)} \frac{dx}{x^{1-\sigma}} + [\xi(t)]^{2\sigma} \int_{\xi(t)}^{\infty} \frac{dx}{x^{1+\sigma}} \\ &= \frac{[\xi(t)]^\sigma}{\sigma} + \frac{[\xi(t)]^\sigma}{\sigma} \\ &= \frac{2[\xi(t)]^\sigma}{\sigma}, \end{aligned} \quad (26)$$

where we used that $0 < \sigma < 1$. Since $N(t) \sim t^{1+\eta}$, we have thus [9]

$$z = \frac{1 + \eta}{\sigma}. \quad (27)$$

For $\sigma \rightarrow 1$ this gives $\xi(t) \sim t^{1+\eta}$ as found in Sec. III, while it gives $z \rightarrow \infty$ for $\sigma \rightarrow 0$, indicating that in this limit $\xi(t)$ is infinite and $R(x, t) \sim 1/t$ is a pure power law for all t .

As in the case $\sigma = 1$ discussed in the previous section, we can also measure z directly by measuring the average logarithmic distance of active sites from the origin,

$$X_{\text{act}}(t) \equiv \exp[\langle \rho(x, t) \ln |x| \rangle] \sim t^z. \quad (28)$$

Values obtained in this way are shown in Fig. 20. In this figure we also show the values predicted by Eq. (27), finding perfect agreement.

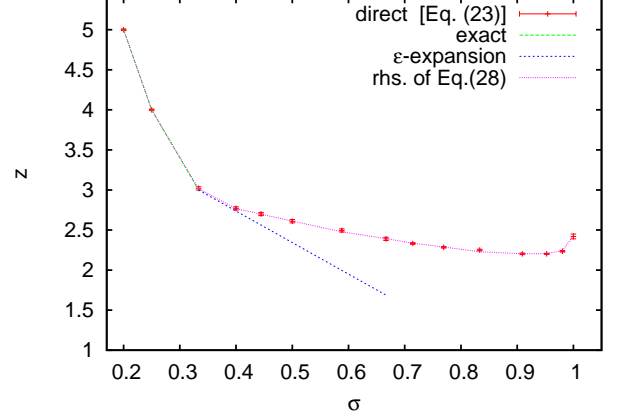


FIG. 20. (Color online) Critical exponent z versus σ . As in Fig. 18, points with error bars are from direct measurements (using now Eq. (28)), while the dotted curve is the prediction from Eq.(27).

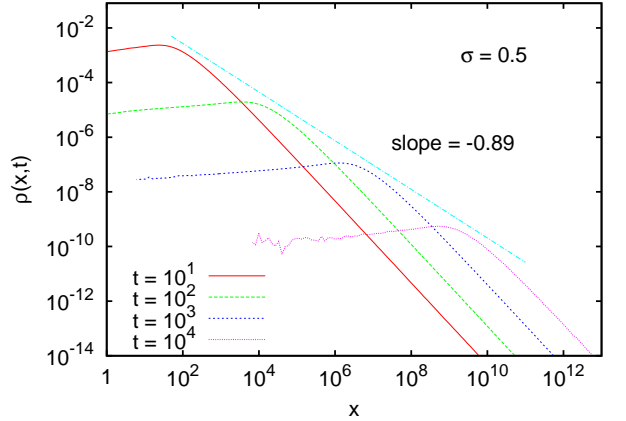


FIG. 21. (Color online) Densities of active sites for critical epidemics with $\sigma = 1/2$, for $t = 10, 10^2, \dots, 10^4$. The straight line has the slope predicted by Eq. (30).

Using Eqs. (24) and (23) we obtain for the density of active sites

$$\rho(x, t) = \frac{x^{\sigma-1}}{t} \Psi(x/\xi(t)), \quad (29)$$

from which we find that $\rho(x, t)$ for fixed t has a peak at $x \approx \xi(t)$ with a height

$$\rho_{\text{max}}(t) \sim t^{-1-(1-\sigma)z} \sim \xi(t)^{\sigma-1-1/z}. \quad (30)$$

This prediction is numerically verified for $\sigma = 0.5$ in Fig. 21.

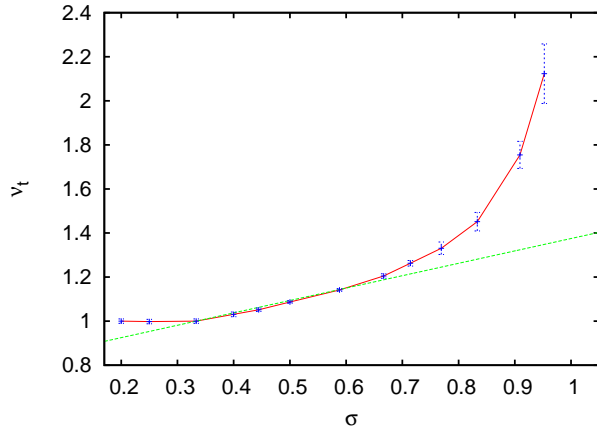


FIG. 22. (Color online) Correlation time exponent ν_t against σ , obtained by data collapse for the number of infected sites. The straight line is the prediction if the ϵ -expansion [9]. For $\sigma < 1/3$, one has the mean field prediction $\nu_t = 1$.

Finally, we can relate the exponents η and δ by a hyperscaling relation as follows: Let us consider the growth of two clusters, one starting at position 0 and the other at x , for some large time t . If $x = \xi(t)$, the probability that they overlap (i.e. have at least one site in common) is of order 1, provided both of them have survived up to t . Thus, up to constants of order one,

$$R(x, t) \sim \xi(t)^{1-\sigma} \approx [P(t)]^2 \quad \text{for } x = \xi(t) \quad (31)$$

or

$$\xi(t)^{\sigma-1} \sim t^{(\sigma-1)z} \sim t^{-2\delta}, \quad (32)$$

which gives [9, 10]

$$\delta = \frac{1}{2}(1-\sigma)z = \frac{1}{2\sigma}(1-\sigma)(1+\eta). \quad (33)$$

Like other hyperscaling relations, it only holds up to the critical dimension, which in the present case means that it holds for $\sigma \geq 1/3$. For $\sigma < 1/3$ the clusters are so sparse that they overlap with probability $< O(1)$. Again, this prediction is satisfied for all tested values of σ .

As in other critical phenomena, there is one other independent critical exponent that governs the behavior for $k_{\text{out}} \neq k_c$ but $k_{\text{out}} \rightarrow k_c$. Traditionally, for percolation with local contacts this can be either the order parameter exponent β or the correlation length exponent ν (for definitions and relations between them, see e.g. [36] or [10]). We use here the correlation time exponent ν_t , which is informally defined via the scaling of a characteristic time scale $\tau \sim |k_{\text{out}} - k_c|^{\nu_t}$. Using this together with the FTS ansatz Eq. (9), we can then determine numerical values of ν_t by plotting $t^\delta n(t)$ versus $(k_{\text{out}} - k_c)t^y$ for different trial values of y . Data collapse should occur for large t

and finite $(k_{\text{out}} - k_c)t^y$, when $y = 1/\nu_t$. Values obtained in this way are shown in Fig. 22. We again see that the mean field prediction $\nu_t = 1$ for $\sigma < 1/3$ is satisfied, and that the ϵ -expansion [9] is correct for σ slightly larger than $1/3$. For $\sigma \rightarrow 1$ one finds that ν_t diverges, which is in agreement with the prediction [30, 31, 33] that the transition is of BKT type for $\sigma = 1$.

As a last remark we should point out that the theoretical discussion of the present section applies only to infinite systems. For critical phenomena with short range interactions, the correlation length ξ describes both what happens in finite systems and, in infinite systems, at finite times or finite distances from the critical point. In the present case, due to the definition of ξ via a geometric average, it is less clear how it relates to the finite system size behavior.

V. SUPERCRITICAL EPIDEMICS WITH $0 < \sigma < 1$

In contrast to the critical case and to the case with $\sigma = 1$, where the epidemics are described by scaling laws, the situation seems much less clear for supercritical epidemics with $0 < \sigma < 1$.

In this case mean field theory predicts for both models exponential growth of $N(t)$ and of the spatial extent [21, 25]. The reason is very simple. For $\sigma < 1$ the wave of infection propagates, in mean field theory, like a ‘pulled’ [23] front, i.e. the growth of the cluster is mainly controlled by its most advanced ‘avant garde’ (for $\sigma > 1$, in contrast, we have seen that the front is ‘pushed’ by the region where the density is large). In this region ahead of the main front the density is very small, and thus saturation effects are negligible. Practically every attempted infection also succeeds, and thus the density increases exponentially with time as

$$R \sim k_{\text{out}}^t \quad (\text{for fixed large } x) \quad (34)$$

Together with the spatial power law $R \sim x^{-1-\sigma}$ this means that an effective front position $x_{\text{front}}(t)$, defined by

$$R(x_{\text{front}}(t), t) = \text{const}, \quad (35)$$

must advance exponentially, like [21]

$$x_{\text{front}}(t) \sim k_{\text{out}}^{t/(1+\sigma)}. \quad (36)$$

As we have seen in Sec. II, this is *not* supported by our data.

The argument leading to Eq. (36) was criticized in [26], who argued that the advance of the front should be linear in time. Unfortunately, this is not supported by the data either, and it is easy to see why. In [26] it was assumed that new infections are not successful, if they appear in regions with extremely small density. This would be correct, if we had assumed *cooperativity* (or ‘synergy’) in the

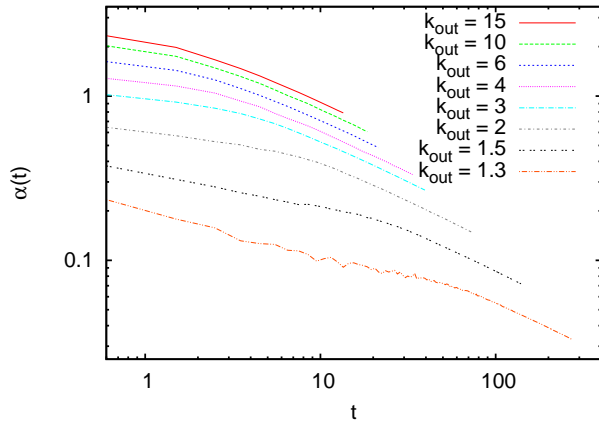


FIG. 23. (Color online) Log-log plot of growth rates (as defined in Eq. (37)) for $\sigma = 0.5$, and for different values of k_{out} . In all cases, the measured growth rates are much smaller than those predicted by Eq. (38), except for very small t .

infection [4, 37]. But this was not assumed in [21, 25], nor was it stated explicitly in [26]. It is also not assumed in the present paper.

We claim that the problem is, instead, a break-down of mean field theory. It is true that the front is pulled, and it is true that the *average* density, averaged over the entire ensemble, is small in the tail of the front. But as soon as a site far ahead of the previous front (i.e., in a region with very small density) is infected, it will generate its own little ‘colony’ and create locally a spot with high density. Thus, in spite of the very small average densities, there will always be non-negligible saturation effects due to the not-so-small *actual* densities.

Let us define a time dependent growth rate $\alpha(t)$ by

$$\alpha(t) = \ln \left[\frac{n(t+1/2)}{n(t-1/2)} \right]. \quad (37)$$

Growth rates for $\sigma = 0.5$ and different values of k_{out} are shown in Fig. 23. According to Eq. (36) we should expect

$$\alpha(t) = \alpha_{\text{mf}}(t) \equiv \frac{\ln k_{\text{out}}}{1 + \sigma}, \quad (38)$$

but we see that the measured α drops, for all tested values of k_{out} , far below this mean field value. Instead, it seems that $\alpha(t)$ decreases for large t like a power

$$\alpha(t) \sim \alpha_0 t^{\gamma-1}, \quad (39)$$

where α_0 depends on k_{out} , but γ is independent of k_{out} . In particular for $\sigma = 0.5$, we obtain $\gamma = 0.49(2)$.

This means that for large t

$$n(t) \sim e^{bt^\gamma} \quad (40)$$

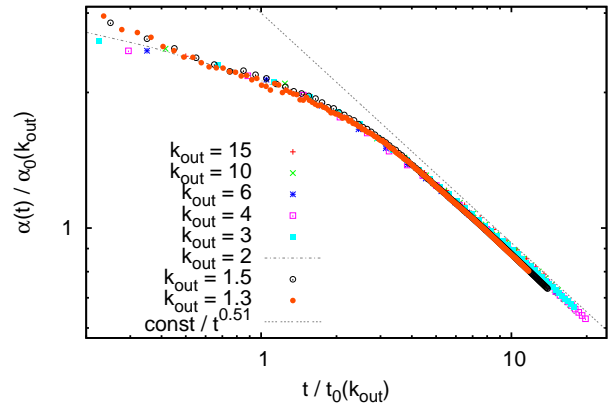


FIG. 24. (Color online) Log-log plot of re-scaled growth rates against re-scaled time. The straight line corresponds to $\gamma = 0.49$.

with $b = \alpha_0/\gamma$, e.g. for $\sigma = 0.5$ we have a stretched exponential with exponent $0.49(2)$. This is particularly evident if we collapse these data onto a single curve by rescaling t and α by arbitrary functions of k_{out} , see Fig. 24.

The value $\gamma = 0.49$ is to be compared with Sec. II, where we obtained an exponent $0.59(1)$ by a straightforward fit. The discrepancy between these two estimates results from systematic deviations from a pure stretched exponential, which are indeed visible in both Figs. 5 and 23. In both cases the curves bend downward (instead of being straight as for clean stretched exponentials), indicating that a naive fit overestimates the growth. Thus it seems likely that the present estimate obtained via the growth rate is more reliable. In addition, we made similar fits with $n(t)$ replaced by $N(t)$. Both should satisfy asymptotically the same stretched exponential, but with different power prefactors. The estimate of γ via the growth rate seems more robust than the direct estimate of Sec. II. Finally, we estimated by both methods (direct fit & growth rate) the exponents for trial functions of the type $f(x) = x^a \exp(bt^\gamma)$ with various (positive and negative) prefactor powers. In most cases the growth rate method gave better results.

For other values of σ , very similar results were found. In particular, the exponent γ is also independent of k_{out} within the estimated errors [39], suggesting that it really depends only on σ . The values obtained in this way for both models are shown in Fig. 25. We see that both models give very similar results. Both are consistent, within the errors, with $\gamma = 1 - \sigma$, but it seems that this is not the correct behavior. A percolation model very similar to the static part of model (A) was studied rigorously by Biskup [38, 40]. He obtained results for the graph diameter of clusters embedded in large but finite

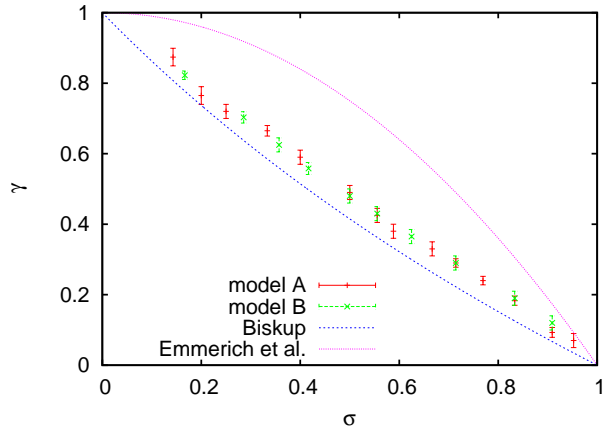


FIG. 25. (Color online) Stretched exponential powers as a function of σ for models (A) and (B). The continuous curves are the predictions of Biskup [38] (lower curve) and Emmerich *et al.* [19] (upper curve).

lattices [40] and for the average graph distance between nodes with large Euclidean distance on infinite lattices [38]. Neither of this is precisely what is measured in the present work, but his results strongly suggest that

$$\gamma = \frac{\ln 2}{\ln \frac{2}{1+\sigma}}. \quad (41)$$

This prediction is also shown in Fig. 25. It agrees reasonably well with our simulations. The simulations are systematically too high, indicating that we have still substantial finite cluster size corrections. Notice that naive fits like Fig. 5 would give even larger estimates.

The graph diameters of graphs embedded in finite lattices were also measured by [19, 41]. Unfortunately, these authors used a rather complicated algorithm which prevented them from using very large lattices and from obtaining high statistics. It also introduced particularly large finite lattice corrections, and the data were analyzed by fitting stretched exponentials directly via plots like Fig. 5. It is presumably for these reasons that [19, 41] obtain $\gamma = 1 - \sigma^2$ (in our notation), which is clearly incompatible with our data and with the prediction of [38, 40] (see Fig. 25) [42].

Figure 3 suggests a scaling ansatz

$$R(x, t) = \phi(x/\xi(t)) \quad (42)$$

similar to Eq. (14), but with $\xi(t)$ being a stretched exponential,

$$\xi(t) \sim N(t) \sim \exp(bt^\gamma), \quad (43)$$

instead of a power law. From this ansatz follows

$$\rho(x, t) = t^{\gamma-1} \psi(x/\xi(t)) \quad (44)$$

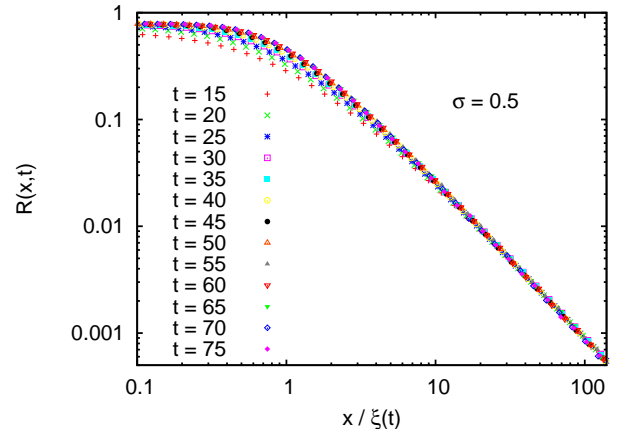


FIG. 26. (Color online) Collapse plot for the data (for $t \geq 15$ only) shown in Fig. 3. We see a perfect data collapse for $t \geq 50$.

where $\psi(z) \propto -z^{-1} \phi'(z)$. This means in particular that $\rho_{\max}(t)$, defined in Eq. (18), decreases like a power of t ,

$$\rho_{\max}(t) = t^{\gamma-1}. \quad (45)$$

This is easy to understand. As we pointed out already at the beginning of this section, the effective growth rate decays as $t^{\gamma-1}$, because new attempted infections are increasingly more likely to target sites that are no longer susceptible. But there it applied to the ‘front of the front’, while here we see that it applies also to the ‘core of the front’ where most of the mass growth occurs. We can interpret Eq. (45) also as a manifestation of a weak sort of ‘self-organized criticality’ [43] in the sense that the speed of growth is such that the density at the front $x \approx \xi(t)$ converges exactly to its critical value.

Equations (45) and (43) together imply the remarkable relation

$$\frac{\log \xi(t)}{\rho_{\max}(t)} \sim t, \quad (46)$$

which should hold for any value of $\sigma \in [0, 1)$ and does not involve σ or γ explicitly.

Equations (42) to (46) are tested numerically, again for $\sigma = 0.5$ and $k_{\text{out}} = 2$, in Figs. 26 to 28. In Fig. 26 we see a perfect data collapse for sufficiently large t , while we see in Fig. 27 that

$$\rho_{\max} = \xi^{-\beta} \quad (47)$$

with $\beta = 0.037$ seems to fit the large time asymptotics. Together with Eq. (43), this would however imply that $\rho_{\max}(t)$ decreases with t faster than a power, which is incompatible with Eq. (45). Therefore we show in Fig. 28 the ratio $\frac{\log \xi(t)}{\rho_{\max}(t)}$ as a function of t , in order to test

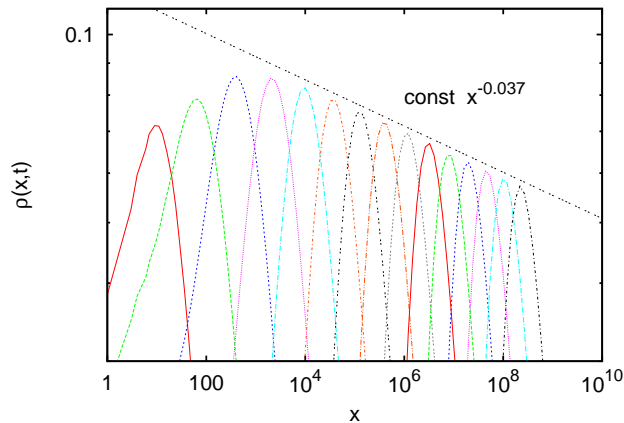


FIG. 27. (Color online) Enlargement of part of Fig. 2. It shows that the peak heights decrease with t , if $t > 20$. For very large t , where Fig. 26 shows a data collapse, this decrease is compatible with a power law $\rho_{\max} \sim \xi^{-\beta}$ with very small β , but we shall argue that this dependence is actually logarithmic.

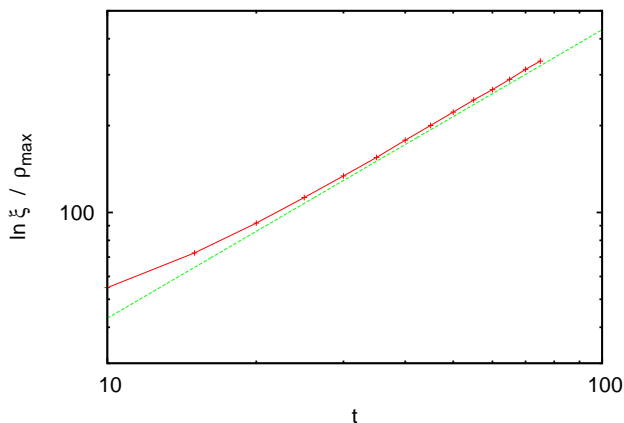


FIG. 28. (Color online) Log-log plot of ρ_{\max} , $\ln \xi$, and of $\ln \xi / \rho_{\max}$ against t . According to Eq. (46) the latter should be proportional to t in the large t limit, which according to Fig. 26 should be reached for $t \approx 50$. The straight line has slope 1.

Eq. (46). Here, $\xi(t)$ is as obtained in the collapse shown in Fig. 26. This defines $\xi(t)$ only up to a constant. This constant (used, by the way, also in Fig. 26) is fixed so that a straight line is obtained in Fig. 28. We see that the data follow indeed a nice linear relationship, showing that at least the entire scheme is internally consistent.

Finally, before leaving this section, let us point out that the scaling relation (42) sets in very late when $k_{\text{out}} \approx k_c$,

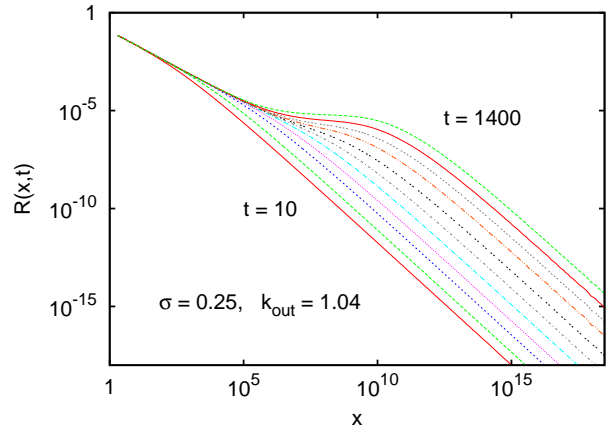


FIG. 29. (Color online) Log-log plot of $R(x, t)$ versus x , for $t = 10, 20, 50, 100, 200, 350, 550, 800, 1000, 1200,$ and 1400 . Control parameters are $\sigma = 0.25$ and $k_{\text{out}} = 1.04$. The latter is ca 20% above k_c .

in particular when $\sigma < 1/3$. In this range of σ , mean field theory holds for $k_{\text{out}} = k_c$, but it does not hold for any $k_{\text{out}} > k_c$. Thus, the cross-over from mean-field to ‘semi-local’ behavior has to happen in a very narrow region with $k_{\text{out}} - k_c \ll 1$. We illustrate this with Fig. 29, where we show $R(x, t)$ for $\sigma = 0.25$ and $k_{\text{out}} = 1.04$ versus x for different values of t , in a way completely analogous to Fig. 3 (where $\sigma = 0.5, k_{\text{out}} = 2$). Instead of the structureless curves in Fig. 3, we see now that for short times the system behaves as if it were critical and mean field. For $t > 200$ it becomes clear that the process is supercritical, but newly infected sites are very far from the seed. It is only for $t > 1000$ that the density starts to grow again appreciably at intermediate distances $x \approx 10^6$, in order to reach finally its asymptotic value $O(1)$.

VI. DISCUSSION AND CONCLUSIONS

Networks embedded in space with connections which preferentially link close neighbors but have also non-vanishing chances to link nodes far apart have numerous applications, from biology to social sciences. Very early it was already proposed to model the link length distribution by power laws [8, 44]. In the present paper we generate such networks by epidemic processes with power behaved distributions for contacts, i.e. infections occur over distances x whose probability decays as $P(x) \sim 1/x^{1+\sigma}$.

While the case of two spatial dimensions will be treated in a forthcoming paper [35], we restricted ourselves here to $d = 1$. This is of course less interesting from the point of view of applications, but it allows much more detailed and precise analysis. Our results concern mainly three different regimes:

- (i) critical epidemics with $0 < \sigma < 1$,
- (ii) epidemics with $\sigma = 1$,
- (iii) supercritical epidemics with $0 < \sigma < 1$.

In all three cases we obtain significant new results, by using simulations on unprecedentedly large sizes. Using hashing, the lattices we used have $2^{64} \approx 1.8 \times 10^{19}$ sites. Such large lattices are needed in order to avoid finite size effects, in view of infections that can spread over billions of sites in one time step.

For critical epidemics we verify predictions from field theory and show that there is one independent critical exponent less than for critical epidemics with short range contacts in ≥ 2 dimensions (in $d = 1$, epidemics with short range contacts die out). For supercritical epidemics with $\sigma = 1$ we verify old predictions based on the Fortuin-Kasteleyn connection between percolation and Potts models. And for supercritical epidemics with $0 < \sigma < 1$ we verify predictions [38, 40] that they lead to ‘medium-size world’ networks, i.e. to networks that are not ‘small world’ in the sense that their size grows exponentially with their graph diameter, but which are also not fractal in the sense that this mass grows like a power. Instead, it grows like a stretched exponential. Related to this is the observation that supercritical epidemics with $0 < \sigma < 1$ spread neither with fixed nor with exponentially increasing velocity, in contradiction to previous claims.

In all three cases we find several new scaling laws that are strongly suggested numerically and which we show in some cases to satisfy non-trivial consistency relations, but for which we do not give theoretical derivations. The need to provide these proofs is one of the main open problems.

In particular, we verify numerically that percolation with $P(x) \sim 1/x^2$ is discontinuous in one dimension, as

proven in [33, 45]. It is intriguing that percolation is also discontinuous in the model of Boettcher *et al.* [46], which can also be understood as a $1 - d$ lattice with additional long range links whose number decreases with x in the same way. The main difference between the two models is that the long range links in the Boettcher model are less random (their lengths can only be a power of 2, and they attach only to selected sites). It would be of interest to check whether the transition in the Boettcher model is also BKT-like as regards the increase of mass of supercritical clusters with their graph diameter.

Finally, a last problem which we left open is finite size behavior. Our strategy was to use lattice sizes which are big enough so that finite (lattice-)size effects can be safely neglected. In view of the interplay between the length scales set by the lattice size, the critical correlation length, and the large contact distances, we may expect finite size effects to be not as simple as in conventional finite size scaling for critical phenomena with short range interactions.

ACKNOWLEDGEMENTS

For very helpful discussions I want to thank Aicko Schumann and Deepak Dhar. I also want to thank the latter for the kind hospitality at the Tata Institute of Fundamental Research in Mumbai, where part of this work was done, and for carefully reading the manuscript. The work was begun at the Complexity Science Group at the University of Calgary, which I also want to thank for generous grant of computer time. Finally my thanks go to Haye Hinrichsen and Hans-Karl Janssen for illuminating correspondence, and to an anonymous referee for pointing out the similarity with Ref. [46].

-
- [1] P. Grassberger, *Math. Biosc.* **63**, 157 (1983).
 - [2] M. E. J. Newman, *Phys. Rev. E* **66**, 016128 (2002).
 - [3] H.-K. Janssen, M. Müller, and O. Stenull, *Phys. Rev. E* **70**, 026114 (2004).
 - [4] G. Bizhani, M. Paczuski, and P. Grassberger, *Phys. Rev. E* **86**, 011128 (2012).
 - [5] D. Achlioptas, R. M. D’Souza, and J. Spencer, *Science* **323**, 1453 (2009).
 - [6] F. van Wijland, K. Oerding, and H. J. Hilhorst, *Physica A* **251**, 179 (1998).
 - [7] H. Grassberger, P. Chaté and G. Rousseau, *Phys. Rev. E* **55**, 2488 (1997).
 - [8] P. Grassberger, “Spreading of epidemic processes leading to fractal structures,” in *Fractals in Physics*, edited by L. Pietronero and E. Tosatti (Elsevier, 1986) p. 273.
 - [9] H.-K. Janssen, K. Oerding, F. van Wijland, and H. J. Hilhorst, *Eur. Phys. J. B* **7**, 137 (1999).
 - [10] F. Linder, J. Tran-Gia, S. R. Dahmen, and H. Hinrichsen, *J. Phys. A* **41**, 185005 (2008).
 - [11] Such a large lattice cannot of course be stored explicitly in the computer memory. Instead we used hashing, implemented using linked lists, with a hash function $h(i) \equiv i \bmod 2^m$ with $m \approx 20 - 30$. For a previous implementation and details, see e.g. [47].
 - [12] D. J. Watts and S. H. Strogatz, *Nature* **393**, 440 (1998).
 - [13] J. Kleinberg, in *Proceedings of the thirty-second annual ACM symposium on Theory of computing*, STOC ’00 (ACM, New York, NY, USA, 2000) pp. 163–170.
 - [14] I. Benjamini and N. Berger, *Rand. Struct. Alg.* **19**, 102 (2001).
 - [15] D. Coppersmith, D. Gamarnik, and M. Sviridenko, *Rand. Struct. Alg.* **21**, 1 (2002).
 - [16] C. F. Moukarzel and M. Argollo de Menzes, *Phys. Rev. E* **65**, 056709 (2002).
 - [17] P. Sen and B. Chakrabarti, *J. Phys. A* **34**, 7749 (2001).
 - [18] R. Juhász, (2012), arXiv:1110.4222v2.
 - [19] T. Emmerich, A. Bunde, S. Havlin, Li Guanlian, and Li Daqing, (2012), arXiv:1206.5710.
 - [20] We avoid this name, in order to avoid confusion with the well established topological dimension discussed, e.g. in [48].

- [21] R. Mancinelli, D. Vergni, and A. Vulpiani, *Europhys. Lett.* **60**, 532 (2002).
- [22] L. S. Schulman, *J. Phys. A* **16**, L639 (1983).
- [23] U. Ebert and W. van Saarloos, *Physica D* **146**, 1 (2000).
- [24] P. Grassberger and W. Nadler, (2000), arXiv:cond-mat:0010265.
- [25] D. del Castillo-Negrete, B. A. Carreras, and V. E. Lynch, *Phys. Rev. Lett.* **91**, 018302 (2003).
- [26] D. Brockmann and L. Hufnagel, *Phys. Rev. Lett.* **98**, 178301 (2007).
- [27] D. Ruelle, *Statistical Mechanics: Rigorous Results* (Benjamin, 1969).
- [28] F. J. Dyson, *Commun. Math. Phys.* **91**, 212 (1969).
- [29] P. W. Anderson, G. Yuval, and D. R. Hamann, *Phys. Rev. B* **1**, 4464 (1970).
- [30] D. J. Thouless, *Phys. Rev.* **187**, 732 (1969).
- [31] J. Cardy, *J. Phys. A* **14**, 1407 (1981).
- [32] C. M. Fortuin and P. W. Kasteleyn, *Physica* **57**, 536 (1972).
- [33] M. Aizenman and C. M. Newman, *Commun. Math. Phys.* **107**, 611 (1986).
- [34] S. N. Dorogovtsev, A. V. Goltsev, and J. F. F. Mendes, *Phys. Rev. Lett.* **96**, 040601 (2006).
- [35] P. Grassberger, (2013), to be published.
- [36] D. Stauffer and A. Aharony, *Introduction to percolation theory* (Taylor & Francis, 1994).
- [37] F. J. Pérez-Reche, J. J. Ludlam, S. N. Taraskin, and C. A. Gilligan, *Phys. Rev. Lett.* **106**, 218701 (2011).
- [38] M. Biskup, *Ann. Prob.* **19**, 2938 (2004).
- [39] This is very clearly seen for $\sigma \approx 1$, where also Eq. (39) holds already for small t . For $\sigma \approx 0$ Eq. (39) holds only for very large t , and the fitted values of γ decrease weakly with k_{out} . We interpret this as a finite-size artifact.
- [40] M. Biskup, (2009), arXiv:math:0406379v2.
- [41] K. Kosmidis, S. Havlin, and A. Bunde, *Europhys. Lett.* **82**, 48005 (2008).
- [42] I might also add that, based on the same model, it is claimed in [19, 49] that such networks embedded in d Euclidean dimensions have in general fractal dimension (as measured via the Euclidean distance) $d_f > d$. This is of course impossible, as it would violate one of the most basic properties of any fractal [50].
- [43] P. Bak, C. Tang, and K. Wiesenfeld, *Phys. Rev. Lett.* **59**, 381 (1987).
- [44] D. Mollison, *J. R. Stat. Soc. B* **30**, 283 (1977).
- [45] M. Aizenman, J. T. Chayes, L. Chayes, and C. M. Newman, *J. Stat. Phys.* **50**, 1 (1988).
- [46] S. Boettcher, V. Singh, and R. M. Ziff, *Nature Communications* **3**, 787 (2012).
- [47] P. Grassberger, *Phys. Rev. E* **67**, 036101 (2003).
- [48] K. Menger, *Dimensionstheorie* (Teubner, Leipzig, 1928).
- [49] Li Daqing, K. Kosmidis, A. Bunde, and S. Havlin, *Nature Physics* **7**, 481 (2011).
- [50] K. J. Falconer, *The geometry of fractal sets* (Cambridge University Press, 1985).